# Combined effects of heterogeneity, anisotropy, and saturation on steady state flow and transport: A laboratory sand tank experiment

Nadia Ursino,[1] Thomas Gimmi, and Hannes Flühler

Soil Physics, Swiss Federal Institute of Technology Zurich, Schlieren, Switzerland

**Abstract.** Field soils show rather different spreading behavior at different water saturations, frequently caused by layering of the soil material. We performed tracer experiments in a laboratory sand tank. Such experiments complement and help comprehension of field investigations. We estimated, by image analysis, the first two moments of small plumes traveling through a two-dimensional, heterogeneous medium with strongly anisotropic correlation structure. Three steady state regimes were analyzed. Two main conclusions were drawn. First, low saturation led to very large heterogeneity and to strong preferential flow. Thus the description of the flow paths and the prediction of the solute arrival times require, in this case, more accurate knowledge about the topological structure. Second, saturation-dependent macroscopic anisotropy is an essential element of transport in unsaturated media. For this reason, small structural soil features should be properly upscaled to give appropriate effective soil parameters to be input in transport models.

## 1. Introduction

Thin layering of different origin, nature, and spatial extent and a slanted orientation of the bedding are common characteristics of natural geological formations. Such anisotropic features can be upscaled and expressed with an anisotropic conductivity tensor. Structural heterogeneities can, in general, be treated with a stochastic approach, and transport is often analyzed on the basis of the first and second moments of a plume. To estimate the effect of local layering on flow and transport at different saturation degrees, we packed a sand tank in a way that our model functions similar to a real soil with an artificial structure.

This laboratory experiment was designed to evaluate effective parameters. *Wildenschild and Jensen* [1999] derived effective conductivities and retention curves by analyzing three different realizations of a heterogeneous sand domain in a two-dimensional tank. They found that the behavior of three differently packed tanks were quite similar, suggesting that this kind of system can be represented as a homogeneous domain characterized by effective hydraulic parameters. *Wildenschild and Jensen* [1999] found that (1) heterogeneity causes water to follow increasingly tortuous flow paths with decreasing saturation because it bypasses low-conductivity regions, (2) a lower saturation corresponds to a higher degree of heterogeneity, and (3) fast breakthrough and tailing characterize preferential flow phenomena due to flow in areas of relatively high conductivity and diffusion and entrapment in poorly accessible zones. The focus of our analysis was on the interplay of three elements: an anisotropic structure, its nonhorizontal bedding, and different saturation conditions. The parameters we intend

to evaluate are the anisotropy of the conductivity tensor and the covariance tensor of solute displacement.

The problem of evaluating effective parameters is linked to the problem of defining the representative elementary volume (REV), being the element over which we average the point properties in order to obtain parameters for the continuum description of our medium [*Bear*, 1972; *Hubbert*, 1956]. If we have information about the structure of the layers and the corresponding materials, we can then choose the scale of definition for our constitutive law, which is the Richards equation. Basically, two approaches are possible to describe flow through a medium with strongly anisotropic structure (small layers of different materials). First, the REV is considered to be smaller than the thickness of the single layer that represents the smallest correlation length. In this case, the correlation structure will be anisotropic, although the conductivities could be locally isotropic. Alternatively, a REV is considered as consisting of many layers. In this case, the REV scale is the scale of a larger correlation length. The correlation structure of a larger, heterogeneous domain consisting of many such REVs can, in this case, be isotropic, and the conductivity will be anisotropic.

For this second approach, i.e., when one uses structural information at a scale that is smaller than the REV scale, one needs upscaling rules. An overview on upscaling is given by *Sanchez-Vila et al.* [1995]. *Desbarats* [1998], for example, addressed the problem of upscaling in the context of discretization of computational domain. He investigated how observations and knowledge of the dynamic processes at the subgrid scale can be upscaled to assign parameters to grid blocks. *Mualem* [1984] proposed a conceptual model for soil made of a large number of very thin layers. According to this model, the effective hydraulic conductivity in the direction parallel and perpendicular to the bedding would correspond to the arithmetic and harmonic mean unsaturated conductivity, respectively. Stochastic models do not always address the upscaling problem. *Yeh et al.* [1985] derived the effective conductivity and its anisotropy ratio for an anisotropic random field and for arbitrary orientation of the mean gradient using a spectral

solution of the first-order stochastic perturbation equation. He found that the variance of capillary pressure head increases with decreasing saturation and that the anisotropy of the effective unsaturated conductivity is strongly dependent on the mean capillary pressure. The theoretical works of *Russo* [1993, 1995a, 1995b] considered solute transport in soils with anisotropic correlation structures and isotropic conductivity tensors. We can assume that for a sand the logarithm of the saturated conductivity, log $K$, and the inverse of the capillary rise $\alpha$ are positively correlated. In this case, *Russo* [1995a] predicts that the longitudinal and the transverse spreading decreases, reaching a minimum, and increases as saturation decreases. For negatively or zero correlated log $K$ and $\alpha$, *Russo* [1995a and 1993] predicts increase of the spreading as saturation decreases. *Russo* [1993, 1995a, 1995b] found that a variable saturation enhances the increase of solute spreading. Concerning the relative orientation of the applied mean gradient and the bedding, when the mean gradient deviates from the main direction of the bedding, the longitudinal component of the covariance displacement tensor decreases, and the transverse component increases [*Russo*, 1995b]. Stochastic models are often limited by a first-order approximation. In general, the conductivity may be characterized by small variabilities only in a given saturation range. Often, for example, under very dry conditions, we predict strong heterogeneity. In this case, the first-order analysis is not rigorously applicable [*Russo*, 1995b].

We performed a tracer experiment on a quasi-two-dimensional random field with a strong anisotropy of the correlation structure, where the applied mean gradient was not parallel to the bedding. The physical model consisted of a tank packed with layers of three different sands. We applied local pulses of a dye tracer as a momentary quasi-point source at 10 different positions and analyzed their behavior at three different flow rates. On the basis of $(x, z)$ images of the 10 dye tracer plumes in the heterogeneous structure we quantified their first and second moments. From the mean trajectories we estimated the anisotropy of the conductivity tensor, and the second moments were interpreted in terms of displacement covariances.

## 2. Material and Methods

### 2.1. Tank Experiment

The sand tank model is one single realization of a two-dimensional anisotropic stochastic formation. Randomly layered cubes of $5 \times 5 \times 5$ cm where prepared from three different sands: a very fine sand ($d = 0.08$–$0.2$ mm), a fine sand ($d = 0.1$–$0.5$ mm), and a coarse sand ($d = 0.3$–$0.9$ mm). Single layers had a thickness of 5 mm. The cubes were saturated, frozen, and then assembled in a polyetilene frame of 75 cm width ($x$), 40 cm height ($z$), and 5 cm depth ($y$) by working in a cold room. All the cubes were rotated at an angle of 45° to the horizontal. Gaps between the cubes and the frame where filled with a mixture of the three sands. A 12 mm thick glass plate covered the frame on both sides. The final result is shown in Figure 1. The packing was homogeneous in the $y$ direction, i.e., perpendicular to the observation surface. For this reason we will refer to the domain as to a quasi-two-dimensional, random, heterogeneous, and anisotropic structure consisting of >1000 rectangular regions 5 cm $\times$ 0.5 cm, each region of very fine, fine, or coarse sand. We interpret the characteristic lengths of a singular rectangular region of the formation as the correlation lengths of the two-dimensional
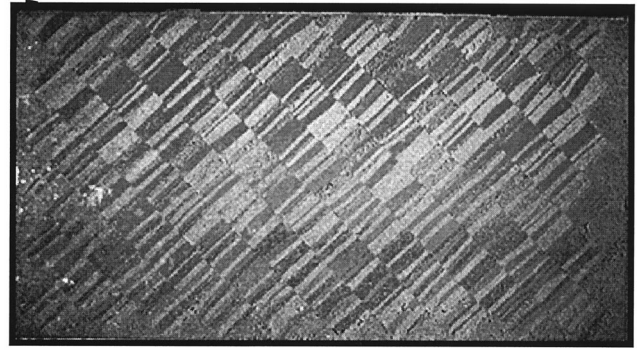


**Figure 1.** Assembled random sand structure.

random field. The anisotropy factor of the structure is 1/10, corresponding to the ratio between the correlation lengths.

Solute transport in this formation was observed at three different mean saturation degrees, which corresponded to the steady states at given water flow rates imposed at the top boundary by a sprinkling bar moving back and forth. We kept the lower boundary at a given negative pressure of $-25$ cm, and we varied the water flux at the top boundary. The angle between the main direction of the bedding and the direction of the applied mean gradient is 45°. The setup of the experimental apparatus is shown in Figure 2.

Our target was to estimate by image analysis the macroscopic anisotropy of the conductivity and the dispersive behavior based on the spatial moments of 10 small solute plumes. The small solute plumes were created by applying pulses of fluorescent dye at 10 different locations on the surface. The dye was applied as an initially frozen cylindrical stick of length 5 cm and diameter 0.5 cm. The dye concentration in the stick was 0.5 g/L. The initial size of the plumes was small compared to the larger correlation length of the formation. As a result of local and larger-scale spreading, the size of the plumes in-
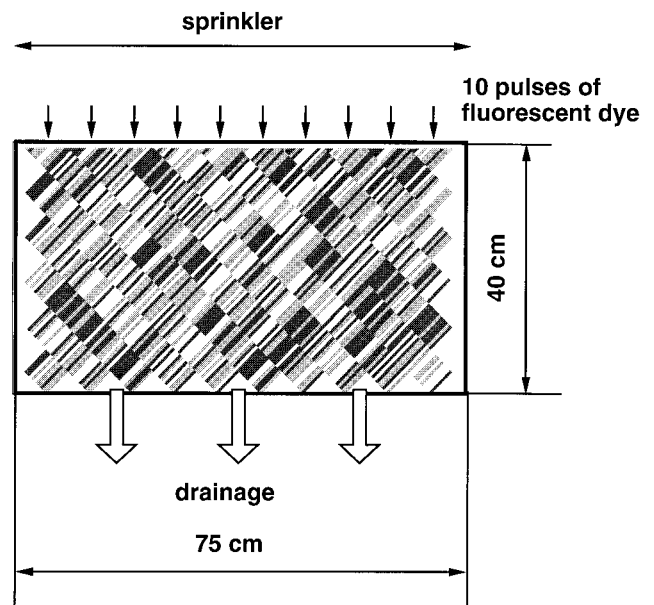


**Figure 2.** Setup of the experimental apparatus and filling pattern of the sand tank as designed by random generation. Coarse sand is dark gray, fine sand is light gray, and very fine sand is white.

creased with time. Nevertheless, each plume was far from ergodic conditions. By averaging the spatial moments of 10 plumes, we obtained parameters that were less affected by local heterogeneity and more representative in a statistical sense.

After applying a dye pulse, pictures of the tank were taken in irregular intervals using a charge-coupled device (CCD) camera. We used Brilliant Sulfaflavine (Sigma Chemical Company, St. Louis, Missouri). Dye molecules were excited by the light of a xenon lamp with a wave length of 420 nm, corresponding to the main excitation wavelength of Sulfaflavine. A filter in front of the camera matched the main emission wavelength of the dye (515 nm) [*Aeby*, 1998]. The resolution of the images was ~225 pixels/cm$^2$.

### 2.2.  Image Analysis

Every digital image, grabbed at time $t$ after the application of the $i$th pulse of dye, is a two-dimensional light intensity function $f_{t,i}(x, z)$. The pictures were corrected for spatially inhomogeneous light conditions. This was done by using the relative intensity distribution obtained from a gray panel in front of the tank, the so-called flat field. After correction, the relation gray level concentration is linear for Brilliant Sulfaflavine in the range of used concentration (below 0.5 g/L) [*Ursino et al.*, 1999]. We set to zero the gray level of pixels with intensity lower than a proper threshold value. This was necessary because pixels which identify location of any dye molecule had a nonzero gray level. We choose the threshold values in order to assure conservation of mass. After correction and thresholding the image of the $i$th plume taken at time $t$ is proportional to the two-dimensional concentration intensity function $C_i(x, z, t)$ of that plume at the given time:

$$f_{t,i}(x, z) \propto C_i(x, z, t). \tag{1}$$

For each time $t$ and plume $i$, we estimated the following parameters: the total mass

$$M_i = \int\int_\Omega C_i(x, z; t)\, dx\, dz, \tag{2}$$

the position of the centroid $[\bar{x}_i(t), \bar{z}_i(t)]$

$$\bar{x}_i(t) = M_i^{-1} \int\int_\Omega x C_i(x, z; t)\, dx\, dz \tag{3}$$

$$\bar{z}_i(t) = M_i^{-1} \int\int_\Omega z C_i(x, z; t)\, dx\, dz, \tag{4}$$

and the components of the covariance tensor of the displacement around the centroid

$$XX_i(t) = M_i^{-1} \int\int_\Omega [x - \bar{x}_i(t)]^2 C_i(x, z; t)\, dx\, dz, \tag{5}$$

$$ZZ_i(t) = M_i^{-1} \int\int_\Omega [z - \bar{z}_i(t)]^2 C_i(x, z; t)\, dx\, dz, \tag{6}$$

$$XZ_i(t) = M_i^{-1} \int\int_\Omega [z - \bar{z}_i(t)][x - \bar{x}_i(t)] C_i(x, z; t)\, dx\, dz, \tag{7}$$

where $\Omega$ is an area delineating the stained plume and an unstained background region in the immediate vicinity of the plume characterized by zero gray level after thresholding. From (1), we can formally substitute $C_i(x, z; t)$ with $f_{t,i}(x, z)$ in (3)–(7).

In our case, the dimension of the plumes is small compared to the correlation length of the soil properties. Thus the spatial moments (3)–(7) of each plume differ because ergodicity is not warranted. In this case, the moments (3)–(7) can be regarded as random variables with their own statistical moments. On the basis of the observation of 10 plumes we can estimate the first and second moments of the centroid displacement and of the spreading around the centroid by evaluating mean and variance of these parameters. The variance of the second moments will not be shown.

The mean centroid trajectory is defined by the coordinates $[\bar{x}(t), \bar{z}(t)]$

$$\bar{x}(t) = \frac{1}{10} \sum_{i=1}^{10} \bar{x}_i(t) - \bar{x}_i(0) \tag{8}$$

$$\bar{z}(t) = \frac{1}{10} \sum_{i=1}^{10} \bar{z}_i(t) \tag{9}$$

being $\bar{z}_i(0) = 0$ for all 10 plumes. The mean components of the covariance tensor of the displacement around the centroid are

$$XX(t) = \frac{1}{10} \sum_{i=1}^{10} XX_i(t), \tag{10}$$

$$ZZ(t) = \frac{1}{10} \sum_{i=1}^{10} ZZ_i(t), \tag{11}$$

$$XZ(t) = \frac{1}{10} \sum_{i=1}^{10} XZ_i(t). \tag{12}$$

Deviation of the centroids' positions from the mean trajectory gives information about ergodicity. In fact, only in the ergodic case does the centroid follow the mean trajectory [*Dagan*, 1991, 1994]. The variances of the horizontal and vertical deviations of the centroids around the mean trajectory var $[\bar{x}(t)]$, var $[\bar{z}(t)]$ were estimated in the following way:

$$\text{var}\,[\bar{x}(t)] = \frac{1}{10} \sum_{i=1}^{10} [\bar{x}(t) - \bar{x}_i(t) + \bar{x}_i(0)]^2 \tag{13}$$

$$\text{var}\,[\bar{z}(t)] = \frac{1}{10} \sum_{i=1}^{10} [\bar{z}(t) - \bar{z}_i(t)]^2. \tag{14}$$

### 2.3.  Macroscopic Anisotropy

Anisotropy $A$ of the conductivity depends on water content in stratified material [e.g., *Mualem*, 1984; *Yeh*, 1985]. If the bedding is not oriented perpendicular or parallel to the mean hydraulic gradient, this anisotropy causes a divergence between the mean centroid trajectory and the direction of the applied mean hydraulic gradient [*Stephens and Heerman*, 1988]. A second consequence of saturation-dependent anisot-
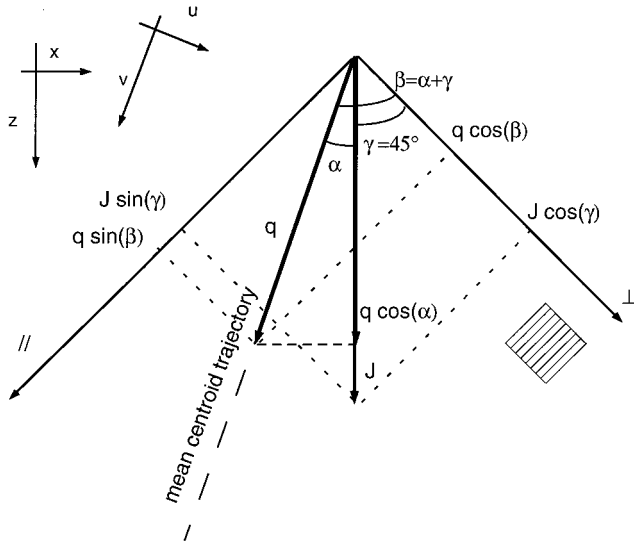
**Figure 3.** Orientation of the hydraulic gradient $J$ and of the mean centroid trajectory (dashed line) with respect to the bedding.



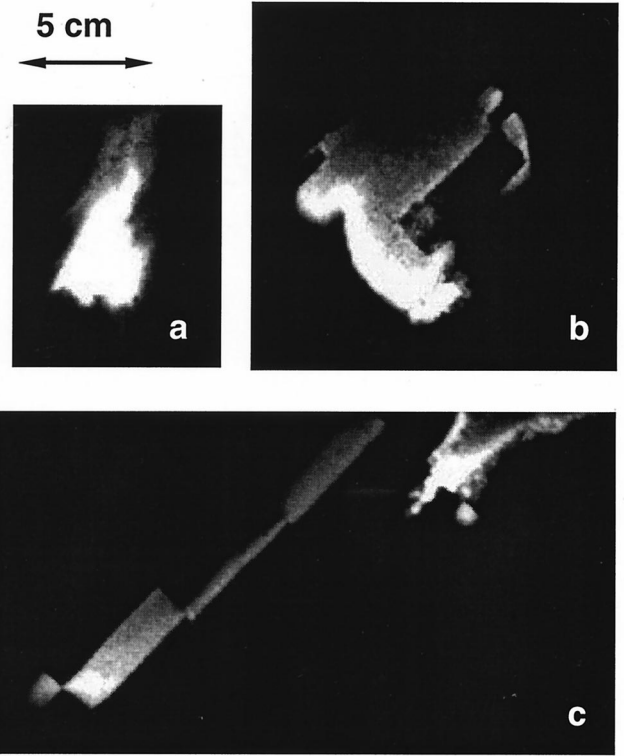**Figure 4.** Typical shape of the plumes when their center of mass was at 10 cm depth. Cases of (a) high, (b) intermediate, and (c) low flow rates.

ropy is that the main axes of a solute plume are not parallel and perpendicular to the main gradient. *Stephens and Heerman* [1988] proposed an expression similar to (15) for evaluating anisotropy of the conductivity tensor $A$ as a function of the divergences between applied gradient, bedding, and mean flow in a horizontally stratified medium. In our case (see Figure 3), the following relation holds:

$$A = K_\parallel / K_\perp = \tan(\beta)/\tan(\gamma), \quad (15)$$

where $K_\perp$ is the conductivity perpendicular to the bedding, $K_\parallel$ is the conductivity parallel to the bedding, $\beta$ is the angle between the direction parallel to the bedding and the mean trajectory, and $\gamma$ is the angle between the direction parallel to the bedding and the vertical direction, the latter being the direction of the applied mean gradient. If $q$ is the centroid velocity along its trajectory, the components of the centroid velocity parallel and perpendicular to the bedding are $q \cos(\beta) = K_\parallel J \cos(\gamma)$ and $q \sin(\beta) = K_\parallel J \sin(\gamma)$. From these, (15) is easily derived. The angle $\alpha$ between the mean trajectory and the mean gradient, which is vertical in our case, was estimated from linear interpolation of the mean trajectory ((8) and (9)).

After estimating the mean trajectories and the components of the covariance tensor of the displacement ((10)–(12)), it is possible to derive the variance of the displacement around the centroid in the direction perpendicular ($UU(t)$) and parallel ($VV(t)$) to the mean trajectory.

$$VV(t) = XX(t) \cos^2(\alpha) + ZZ(t) \sin^2(\alpha)$$
$$- 2XZ(t) \sin(\alpha) \cos(\alpha), \quad (16)$$

$$UU(t) = ZZ(t) \cos^2(\alpha) + XX(t) \sin^2(\alpha)$$
$$+ 2XZ(t) \sin(\alpha) \cos(\alpha), \quad (17)$$

where $\alpha = \gamma - \beta$. The parameters introduced in this section were estimated for three different flow rates that led to three different mean water contents.

## 3. Results

The discharge of the sprinkler $j$ was measured several times during every experiment to check its stationarity. With the horizontal section of the tank $S = 375$ cm$^2$, a flow rate $Q = j/S$ of $5 \times 10^{-6}$, $3 \times 10^{-6}$, and $1 \times 10^{-6}$ m/s was calculated for the three different upper boundary conditions (Table 1). The three different flow rates led to plumes of very different shape, velocity of advancement, and spreading characteristics. Figure 4 shows three typical plumes with the center of mass at 10 cm depth below the tank surface, which were observed at the high (Figure 4a), intermediate (Figure 4b), and low (Figure 4c) flow rates.

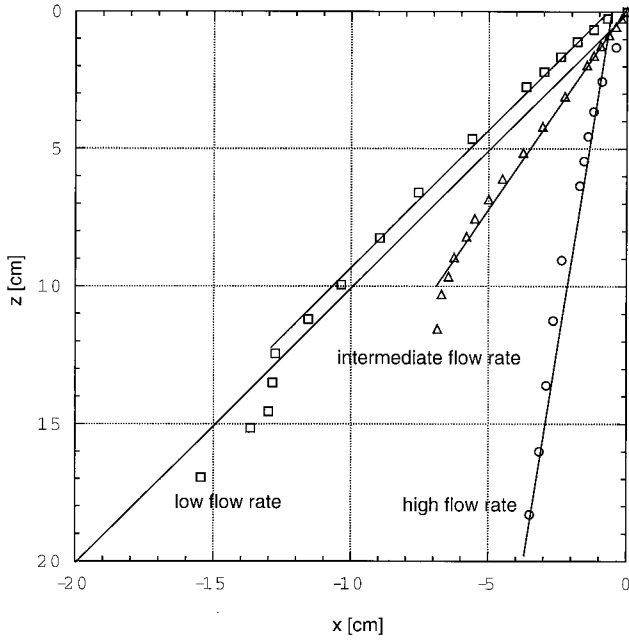Figure 5 shows the mean trajectories for the three flow rates.

**Table 1.** Specific Discharge $Q$, Vertical Component of the Centroid Velocity $q_z$, Ratio Between the Vertical Component of the Centroid Velocity and the Specific Discharge $q_z/Q$, Angle Between the Mean Trajectory and the Vertical $\alpha$, Anisotropy Factor $A$, and Velocity of the Centroid Along the Mean Trajectory $q$ for the Three Different Cases Examined

| $Q$, m/s | $\alpha$, grad | $A$ | $q_z$, m/s | $q_z/Q$ | $q$, m/s |
|---|---|---|---|---|---|
| $5.2 \times 10^{-6}$ | 9.2 | 1.4 | $2.35 \times 10^{-5}$ | 4.5 | $2.38 \times 10^{-5}$ |
| $3.2 \times 10^{-6}$ | 34.4 | 5.3 | $9.57 \times 10^{-6}$ | 3.0 | $1.16 \times 10^{-5}$ |
| $1.3 \times 10^{-6}$ | 44.9 | $5.7 \times 10^2$ | $1.77 \times 10^{-5}$ | 13.6 | $2.50 \times 10^{-5}$ |

**Figure 5.** Trajectories of the centroid for the three different water fluxes. Circles correspond to high flow rate, triangles correspond to intermediate flow rate, and squares correspond to low flow rate.



**Figure 6.** Vertical displacement of the centroid for the three different water fluxes. Circles correspond to high flow rate, triangles correspond to intermediate flow rate, and squares correspond to low flow rate.

They correspond to the sequence of the averaged positions of the centroids estimated by applying (8) and (9). Clearly, saturation has a pronounced effect on the direction of the mean flow. By linear interpolation of the positions of the centroids we derived the angle $\alpha = \beta - \gamma$ (see Figure 3) between the mean trajectory and the vertical. The effective anisotropy of the conductivity, as estimated with (15), increased considerably with decreasing saturation, as shown in Table 1. Figure 6 shows the mean vertical position of the centroid $\bar{z}$ versus time $t$. The slope defines the vertical component of the centroid velocity $q_z = d\bar{z}(t)/dt$ (see Figure 3). The vertical component $q_z$ of the centroid velocity $q$ could be estimated by linearly interpolating the experimental data. The values of $q_z$ and $q_z/Q$ estimated for the three water fluxes are reported in Table 1. The centroid velocity $q = q_z/\cos(\alpha)$ along the mean trajectory was derived from $q_z$ and $\alpha$ (see Figure 3). The results are listed in Table 1. The deviation of the experimental data from the linear trend with depth in Figures 5 and 6 evidences the effect of the lower boundary condition. For the intermediate water flux the lower boundary effect is evident already at the depth of 10 cm.

In Figures 7 and 8 the elements on the diagonal of the displacement covariance tensor, $XX(t)$ (equation (10)) and $ZZ(t)$ (equation (11)), are plotted as a function of the vertical distance traveled by the centroid. In Figures 7 and 8 the sum of the cumulative spreading around the centroid and the variance of the displacement of the centroid around the mean trajectory are also shown, as indicated. The spreading due to nonergodicity of the single plumes is not negligible. It is evident from the results shown here that location and spreading of the plumes is strongly influenced by anisotropy, which causes a deviation of the trajectories from the direction of the applied mean gradient. Given the anisotropy and its effect in terms of the deviation $\alpha$, we can estimate spreading around the centroid in the direction parallel and perpendicular to the mean trajectories, as presented in the previous paragraph. The variances of the
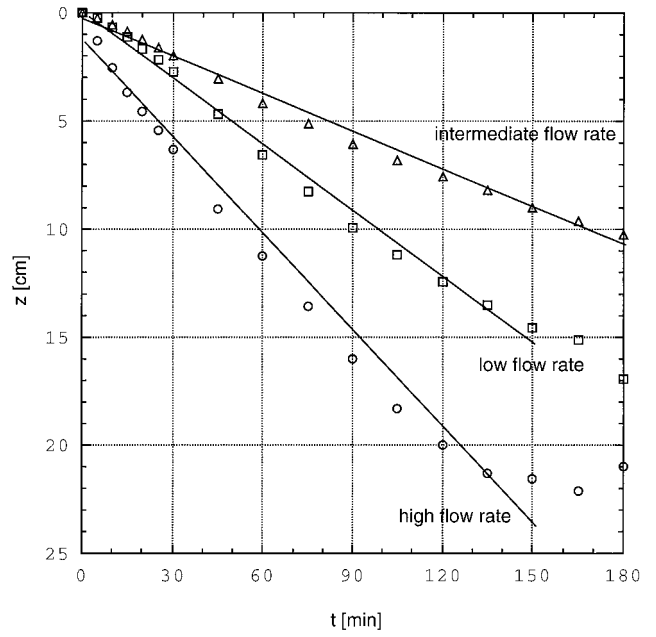
displacements in the direction perpendicular and parallel to the mean trajectory from (16) and (17) are plotted in Figures 9 and 10, respectively, as a function of the vertical centroid displacement.
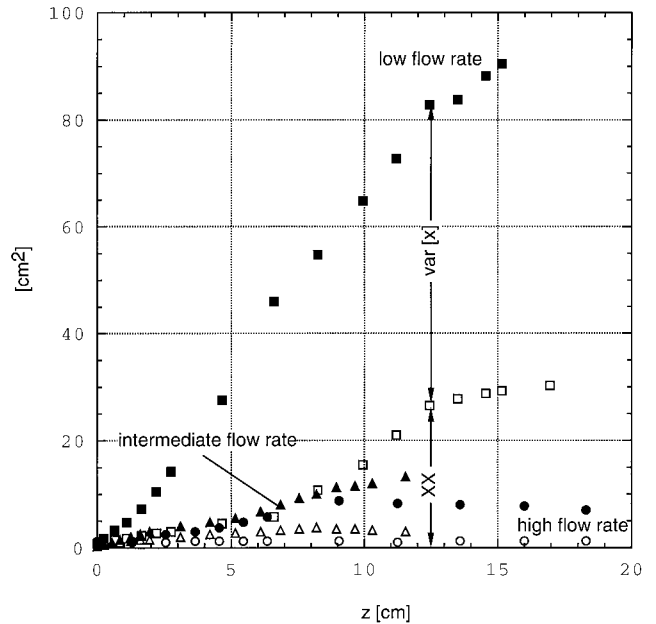


**Figure 7.** Variance of the horizontal displacement around the centroid ((10), open symbols) and of the centroids around the mean trajectories ((13), solid symbols) for the three different water fluxes. The variance of the displacement of the centroid around the mean trajectory is given by the difference between open and solid symbols as indicated. Circles correspond to high flow rate, triangles correspond to intermediate flow rate, and squares correspond to low flow rate.
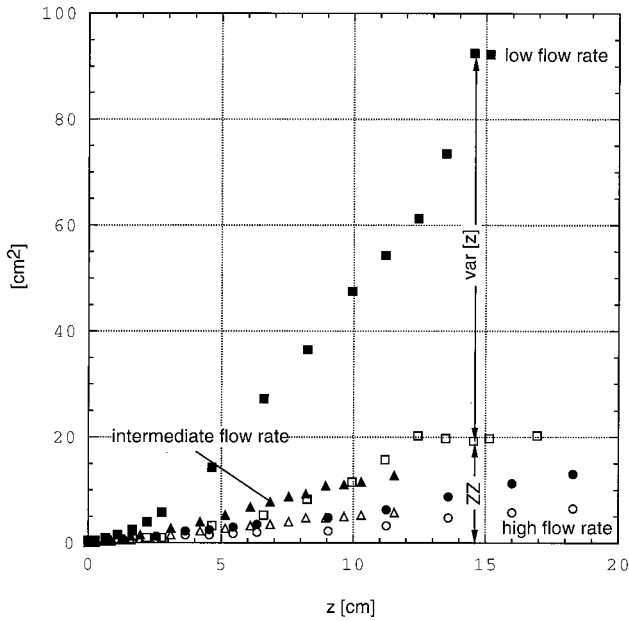
**Figure 8.** Variance of the vertical displacement around the centroid ((11), open symbols) and of the centroids around the mean trajectories ((14), solid symbols) for the three different water fluxes. The variance of the displacement of the centroid around the mean trajectory is given by the difference between open and solid symbols as indicated. Circles correspond to high flow rate, triangles correspond to intermediate flow rate, and squares correspond to low flow rate.

## 4. Discussion

After image analysis, the tank experiment provided a data set that illustrates the behavior of an anisotropic stochastic
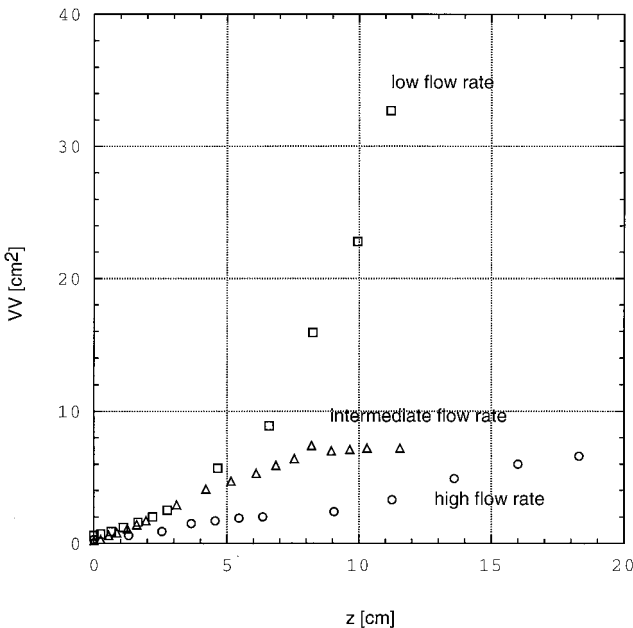


**Figure 9.** Variance of the displacement around the centroid in the direction parallel to the mean trajectory ($VV$, (16)) for the three different water fluxes. Circles correspond to high flow rate, triangles correspond to intermediate flow rate, and squares correspond to low flow rate.



**Figure 10.** Variance of the displacement around the centroid in the direction perpendicular to the mean trajectory ($UU$, (17)) for the three different water fluxes. Circles correspond to high flow rate, triangles correspond to intermediate flow rates, and squares correspond to low flow rate.
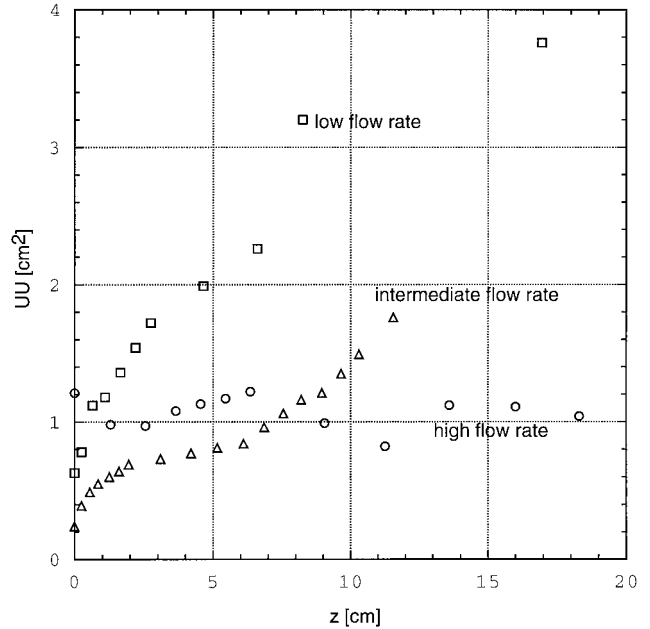
field with respect to flow and transport at three different water fluxes. The data set was condensed to the first and second moments of an "averaged" plume as a function of time, as explained in section 2.2.

From the first moments we could derive information about the effective velocity of the plumes and the anisotropy factor of the conductivity tensor. Increasing the flux, for a constant lower boundary condition, increased the mean water saturation and reduced the anisotropy factor of the conductivity tensor. This can be explained by invoking, for example, the theory of *Mualem* [1984] for soils consisting of many thin parallel layers having different hydraulic properties. The Mualem model shows that owing to the presence of more conductive layers (the coarse material in the saturated case and the fine in the unsaturated one) the degree of anisotropy decreases, attaining a minimum, but increases as the saturation decreases. Our experimental data describe the second phase, where anisotropy increases with decreasing saturation. The increased anisotropy of the conductivity tensor was reflected by a more pronounced deviation of the mean trajectory from the mean gradient in our medium, where the bedding and the mean gradient were not parallel. The deviation of the centroid trajectories from the direction of the vertical gradient could not be predicted by any equivalent homogeneous system.

For the lowest flux at the upper boundary the highest displacement velocity was observed. This was due to a reduction of the active section of the medium available for flow. Figure 6 verifies that even with a more pronounced angle that the trajectory forms, at the lowest flux (see Figure 5) the vertical component of the centroid velocity is larger than at the intermediate flux (see also Table 1). This exceptional increase of the vertical velocity corresponding to a smooth decrement of the water flux indicates that preferential flow develops in case of very low flow rate. We observed then that both $q$ and $q_z$

present a minimum corresponding to the intermediate flow. They decreased first and then increased as the discharge decreased.

According to a mobile-immobile transport model [*Coats and Smith*, 1956], the solute is transported by a convection-dispersion process in the mobile region and also has access to the immobile region by diffusion. The ratio between the vertical component of the centroid velocity and the specific discharge $q_z/Q$, according to a mobile-immobile model when exchange is negligible is inversely proportional to the mobile water content $\theta_m$ (water content of the mobile zone) [*Jury et al.*, 1991]. Astonishingly, $\theta_m$ is larger for the intermediate than for the high flow rate (see $q_z/Q$ in Table 1). The anisotropy ratio is lowest for the high flow rate. Therefore the differences in conductivities are larger for the intermediate than for the high flow rate. Thus the area contributing to flow should be reduced rather than increased for the intermediate as compared to the high flow rate. On the basis of the similarity between Sulfaflavine and Lissamine FF and on literature data [*Smart and Laidlaw*, 1997] we did not expect significant retardation caused by sorption of the dye at our sands. The only possible explanation is a retardation at the intermediate rate by diffusion into zones of essentially immobile water. This immobile water is presumably located in the coarse sand, which is not completely drained but has a very low conductivity at these conditions. The coarse sand is probably more saturated and contributing to flow at the high flow rate and completely dry at the low flow rate when we clearly observe that part of the plumes are blocked in the upper part of the tank (Figure 4c).

The second moments of the plumes were estimated from the spreading around the centroid and spreading of the centroids around the mean trajectories. The physical model reflects the concurrence of all different mechanisms that interact to determine a certain spreading behavior because it is not affected by any simplifying assumption regarding flow and transport processes. It is difficult to distinguish the concurrent causes that determine spreading in our case. This complicates a direct comparison of our experimental results with the theoretical outcomes of the simplified stochastic models. Several elements have to be taken into account to interpret the plots of the second moments. First, pore-scale heterogeneity physically cannot be avoided; it manifests in a supplementary diffusive/dispersive displacement. Second, anisotropy leads to a deviation of the mean trajectory from the direction of the mean gradient (when the bedding is not perpendicular or parallel to the mean gradient) and is dependent on saturation (Figure 5). As a consequence, it is not possible to compare cases of arbitrary variable saturation and direction of the mean trajectory. Third, the dimension of the plumes was comparable with the larger correlation length. A single plume did not represent an ergodic case. As a consequence, the spreading of the particles around the mean trajectory was due to the random displacement of the centroid and to the spreading around the centroid itself. Fourth, owing to the finite size of the physical model and the effect of the lower boundary condition, only a short depth provided information about the behavior of the plumes at a certain saturation degree. Definitely no asymptotic behavior could be observed. Fifth, our observation concerns a single realization with one set of parameters for correlation length and covariance structure that characterize the random distribution of the soil properties. The main focus of the analysis, consequently, switches from the purely stochastic effects of

heterogeneity to the mechanisms that determine the dispersive transport in our system at different saturation degrees. The fourth and the fifth points similarly apply to field observations of transport through the vadose zone from a relatively small source, where the presence of the water table limits the depth of observation to few correlation lengths and the injection source is rather local.

As the water content decreased, the large horizontal spreading (Figure 7, open symbols), as compared to the spreading perpendicular to the mean trajectories (Figure 10), was mainly due to the anisotropy-induced deviation of the trajectories. The differences in terms of spreading between the high and the intermediate flow rates were not relevant if compared with the low flow rate (Figures 9 and 10). The low flow rate led to very high spreading compared to the high and intermediate flow rates. A net of preferential flow paths developed mainly in the fine sand, as shown in Figure 4c. In this case, vertical and horizontal spreading were comparable owing to the fact that the transport developed almost in the direction parallel to the bedding that was at 45° (Figures 7 and 8). In general, we observed that as expected [*Russo*, 1993, 1995a, 1995b], after traveling a short distance, spreading perpendicular to the mean trajectory is ~1 order of magnitude smaller than spreading in the direction of the mean trajectory (Figure 9). Spreading perpendicular to the mean trajectory is the effect of the winding trajectories paths, whereas the spreading in the direction parallel (Figure 10) is mainly due to the variation of the velocity. Both $VV$ and $UU$ are relatively high in the low flow rate case, where trajectories are more tortuous owing to preferential flow compared to the other two.

Finally, the images of three typical plumes for the three different flow rates (Figure 4) suggest some qualitative considerations. It is clear that at the high flow rate the flow paths are not at all tortuous and the structure of the sand layers is barely influencing the plume shape. At the low flow rate, in contrast, the shape of the plume reflects the structure features. The transport behavior appears to be consistently different. Transport occurs mainly in the fine sand, and dye circumvents the regions occupied by the other two sands acting as low conductivity regions. Probably, only by knowing in detail the fine sand structures would it be possible to predict the low-saturation transport regime, and only by performing low flow rate tracer experiments would it be possible to guess the fine-sand structure that is rather invisible at the high flow rate.

## 5. Summary and Conclusions

The aim of the presented experimental study was to estimate the statistical moments of a tracer plume at different water saturations in a given random distribution of formation properties. In a way, this target is comparable to the objective of a stochastic model, except that particles are not driven by numerically computed velocities but by real water flow. In particular, this experiment was focusing on the effects of the following three factors: anisotropic structure, bedding nonperpendicular or nonparallel to the main gradient, and variable mean saturation.

The experimental setup can be analyzed on the basis of two theoretical models: (1) a stochastic field with isotropic correlation structure but anisotropic conductivity tensor (REV should include a certain number of layers) and (2) a stochastic field with an anisotropic correlation structure and an isotropic conductivity tensor, as investigated by *Russo* [1993], 1995a,

1995b]. If one focuses on model 1, anisotropy of the conductivity tensor, the medium properties have to be upscaled to the scale of the longer correlation length of the structure. In this case, one defines the properties of a squared region containing, for instance, 10 different layers, and the (square) REV coincides with this region. Models focusing on upscaling anisotropy at the level of the REV only, by defining appropriate conductivity tensors [*Sanchez-Vila et al.*, 1995; *Desbarats*, 1998], grasp only part of the flow and transport problem. Otherwise, if one focuses model 2 on the properties of each layer, our REV is smaller than the smaller correlation length (depth of a layer), and the description of the structure is more detailed. In the stochastic model of *Russo* [1995b] the transport problem is solved for heterogeneous and anisotropic structures where the mean gradient is inclined relative to the bedding, but this work ignores the case when the direction of the mean trajectory depends on the saturation degree.

Our main results are the following: (1) owing to the saturation dependence of the conductivity tensor the direction of the mean trajectory was not constant for different water fluxes; (2) deviation from the direction of the applied mean gradient increased with decreasing saturation; (3) preferential flow at low saturation dramatically reduced the arrival times of the centroids at a certain depth; (4) longitudinal and transversal spreading were highest at the low saturation.

Our main conclusion is that in cases similar to the one examined, one should consider the effect of saturation on deviation of the mean trajectory first and then on spreading. Thus cases of anisotropic structures with the imposed mean gradient not parallel to the bedding have to be analyzed at two different scales: a scale where the REV includes layers (scale of the larger correlation length) and, eventually, one where the REV is inside a layer (scale of the smaller correlation length). The first approach (REV including many layers) allows the quantification of the anisotropy of the conductivity tensor and the prediction of the angle between the mean trajectory and the applied mean gradient. In our experimental case, the mean trajectory was estimated by image analysis, and the anisotropy of the conductivity tensor for the whole tank was inferred from these data. The second approach (REV inside the layers) led to a more detailed description of the heterogeneous structure. We derived the following inferences from the images of the plumes (Figure 4). At the low flow rate the shape of the plumes contain information about the underlying structure because flow and transport develop through the fine sand only. At the high flow rate we cannot derive this kind of information because the plumes seem to travel through an almost homogeneous and isotropic medium. Then the following open questions arise: (1) Does a first-order analysis apply to the low saturation case or are variances of the parameters too large? (2) In presence of strong anisotropy would it be more meaningful to switch to a two region model, where one region participates to transport and the other one is responsible of retardation and tailing as observed by *Wildenschild and Jensen* [1999]?

## References

Aeby, P. G., Quantitative fluorescence imaging of tracer distributions in soil profiles, *Diss. ETH 12951*, Ph.D. thesis, Eidg. Tech. Hochsc., Zurich, Switzerland, 1998.

Bear, J., *Dynamics of Fluids in Porous Media*, Dover, Mineola, N. Y., 1972.

Coats, K. H., and B. D. Smith, Dead end pore volume and dispersion in porous media, *SPEJ Soc. Pet. Eng. J.*, *4*, 73–84, 1956.

Dagan, G., Dispersion of a passive solute in non-ergodic transport by steady velocity fields in heterogeneous formations, *J. Fluid Mech.*, *233*, 197–210, 1991.

Dagan, G., The significance of heterogeneity of evolving scales to transport in porous formation, *Water Resour. Res.*, *30*(12), 3327–3336, 1994.

Desbarats, A. J., Scaling of constitutive relationships in unsaturated heterogeneous media: A numerical investigation, *Water Resour. Res.*, *34*(6), 1427–1435, 1998.

Hubbert, M. K., Darcy's law and the field equations of the flow of underground fluids, *Trans. Am. Inst. Min. Metall. Pet. Eng.*, *207*, 222–239, 1956.

Jury, W. A., W. R. Gardner, and W. H. Gardner, *Soil Physics*, John Wiley, New York, 1991.

Mualem, Y., Anisotropy of unsaturated soils, *Soil Sci. Soc. Am. J.*, *48*, 505–509, 1984.

Russo, D., Stochastic modeling of macrodispersion for solute transport in a heterogeneous unsaturated porous formation, *Water Resour. Res.*, *29*(2), 383–397, 1993.

Russo, D., On the velocity covariance and transport modeling in heterogeneous anisotropic porous formations, 2, Unsaturated flow, *Water Resour. Res.*, *31*(1), 139–145, 1995a.

Russo, D., Stochastic analysis of the velocity covariance and the displacement covariance tensors in partially saturated heterogeneous anisotropic porous media, *Water Resour. Res.*, *31*(7), 1647–1658, 1995b.

Sanchez-Vila, X., J. P. Girardi, and J. Carrera, A synthesis of approaches to upscaling of hydraulic conductivities, *Water Resour. Res.*, *31*(4), 867–882, 1995.

Smart, P. L., and I. M. S. Laidlaw, An evaluation of some fluorescent dyes for water tracing, *Water Resour. Res.*, *13*(1), 15–33, 1977.

Stephens, D. B., and S. Heermann, Dependence of anisotropy on saturation in a stratified sand, *Water Resour. Res.*, *24*(5), 770–778, 1988.

Ursino, N., T. Gimmi, and H. Flühler, The effect of lower scale anisotropy on transport in unsaturated porous media, in *Modelling of Transport Processes in Soils at Various Scales in Time and Space*, edited by J. Feyen and K. Wiyo, pp. 174–183, Wageningen Pers, Wageningen, Netherlands, 1999.

Wildenschild, D., and K. H. Jensen, Laboratory investigations of effective flow behavior in unsaturated heterogeneous sands, *Water Resour. Res.*, *35*(1), 17–27, 1999.

Yeh, T.-C., L. W. Gelhar, and A. L. Gutjahr, Stochastic analysis of unsaturated flow in heterogeneous soils, 1, Statistically anisotropic media with variable $\alpha$, *Water Resour. Res.*, *21*(4), 457–464, 1985.

H. Flühler and T. Gimmi, Swiss Federal Institute of Technology Zurich, Soil Physics, Grabenstrasse 3, CH-8952, Switzerland.

N. Ursino, Dipartimento di Ingegneria, Idraulica, Marittima e Geotecnica, Universitá di Padova, via Loredan 20, I-35131 Padua, Italy. (nadia@idra.unipd.it)